Microstructure, magnetic and mechanical properties of Ni–Zn ferrites prepared by powder injection moulding

J. Gutiérrez-López [a], E. Rodriguez-Senín [a], J.Y. Pastor [b], M.A. Paris [c], A. Martín [b], B. Levenfeld [a], A. Várez [a,*]

[a] Material Science and Engineering Department, Universidad Carlos III de Madrid, Avda. Universidad, 30. 28911-Leganés, Spain
[b] Departamento de Ciencia de Materiales, Universidad Politécnica de Madrid, ETSI de Caminos, Canales y Puertos. C/ Profesor Aranguren s/n. E28040–Madrid, Spain
[c] Hispanoferritas-Ferroxcube, Polígono Industrial El Henares, Guadalajara, Spain

Keywords:
PIM
Ni–Zn ferrites
Mechanical properties
Magnetic properties

A B S T R A C T

Nowadays, the electronic industry demands small and complex parts as a consequence of the miniaturization of electronic devices. Powder injection moulding (PIM) is an emerging technique for the manufacturing of magnetic ceramics. In this paper, we analyze the sintering process, between 900 °C and 1300 °C, of Ni–Zn ferrites prepared by PIM. In particular, the densification behaviour, microstructure and mechanical properties of samples with toroidal and bar geometry were analyzed at different temperatures. Additionally, the magnetic behaviour (complex permeability and magnetic losses factor) of these compacts was compared with that of samples prepared by conventional powder compaction. Finally, the mechanical behaviour (elastic modulus, flexure strength and fracture toughness) was analyzed as a function of the powder loading of feedstock. The final microstructure of prepared samples was correlated with the macroscopic behaviour. A good agreement was established between the densities and population of defects found in the materials depending on the sintering conditions. In general, the final mechanical and magnetic properties of PIM samples were enhanced relative those obtained by uniaxial compaction.

1. Introduction

Powder injection molding (PIM) is a competitive manufacturing technology for producing geometrically complex parts from a wide range of metallic and ceramic materials [1–12]. The processes including mixing, molding, debinding and sintering are dependent upon the types of binder used. In the mixing step, the powder is dispersed in an organic vehicle, which is called binder. These binders normally are multicomponent systems, composed of a thermoplastic with high molecular size and a second component, constituted by a low molecular size polymer. The first component supplies the strength in the green stage, while the second gives the required flowability to the mixture for the injection purpose. The resulting feedstock (comprising of powder and binder) is then injected into a shape-forming mould cavity. Once obtained the injected parts, named green piece, it is necessary to remove the binder. The debinding step requires the largest processing time and normally in this step most of the defects, such as blistering, cracking and bloating form. In order to reduce the debinding time and to make defect free parts, different debinding techniques have been developed, including thermal, capillary, solvent, catalyzed and subsequent combinations of these. Finally, the debounded part is sintered to achieve the required mechanical properties.

In the particular case of ceramic materials, this process has been widely studied in structural materials such Al_2O_3 [3–5] or ZrO_2 [6–8]; however, few papers about PIM of ferrites have been published [9–12].

In general, PIM parts have better properties than specimens fabricated by conventional powder technology [13]. In the particular case of ferrites, there is scarce information available in the literature, and only exist a few references related to mechanical properties in ferrites [14]. On the other hand, ferrites are soft magnetic ceramic material used in plenty of electronic displays where high permeability and low loss are the main requirement [14]. There are three important types of commercial spinel ferrites: Mn–Zn, Mg–Ni and Ni–Zn; most of these are processed by compaction and extrusion, but nowadays the electronic industry increasingly demands small components with complex geometries.

This experimental work focused on the effect of the sintering temperature on the microstructure and magnetic behavior (initial permeability and magnetic losses) of Ni–Zn specimens prepared by powder injection molding. The effect of the powder loading of feedstock on the mechanical properties of this ferrite has been carried out. For every experimental condition, all the properties of PIM samples studied have been compared with those of uniaxially compacted specimens.

2. Experimental procedure

2.1. Materials

The starting raw material was a granulated pre-sintered Ni–Zn Ferrite powder which is normally used for the industrial manufacturing of ferrites by uniaxial pressure. This powder is a pre-sintered mixture of Fe_2O_3, NiO and ZnO. SEM images show that the powder is heavily agglomerated (5–500 μm) in large spheres (Fig. 1). The binder used was a multicomponent system with two components: a backbone polymer that provides strength, and a low molecular weight component, which provides high flowability to the binder, decreasing the viscosity at the processing temperature.

2.2. Processing and experimental techniques

Two different manufacturing ways were used: powder injection moulding and uniaxial compaction. In the case of PIM, powder-binder mixtures were prepared by a twin-screw extruder Thermohaake Rheomex CTW100p with a temperature profile of 160–165–170 °C and a screw speed of 40 rpm. Before the mixture was introduced into the extruder, all the constituents were pre-mixed in a turbula mixer for 30 min. Three mixtures with different powder volume fractions were prepared (52, 55 and 58%) in the same conditions of temperature and screw speed. After extrusion samples were pelletized for use in an injection machine Arburg 220 S 250–60. The injection process was performed in a mould composed of 2 simple pieces: 3-point bend (for mechanical testing) and toroid (for magnetic measurements) parts, with volumes 2.28 and 0.84 cm^3 respectively. Prior to the sintering process, the polymeric part was removed by a combination of solvent and thermal debinding.

The uniaxial compaction specimens were fabricated with a dual effect pressing and 100 MPa of pressure, comparable with industrial conditions. The specimens were fabricated for three points bending test and in toroid form to measure the magnetic properties.

Finally, the toroidal specimens were sintered in air at different temperature, from 900 °C to 1300 °C for measurement of density and magnetic properties, and to observe the evolution of the microstructure. Three point bend specimens were sintered in air at 1250 °C to evaluate the mechanical properties. The sintered densities were determined using the Archimedes method; the magnetic properties of toroidal specimens (10.31 × 5 × 3.45 mm outer diameter, inner diameter and depth respectively) (initial permeability and loss factor) were measured, as function of frequency, at room temperature with a Hewlett-Packard LCR-meter HP4285A in toroids. Powder X-ray diffraction (XRD) patterns were recorded with Cu Kα radiation in an X'Pert Philips diffractometer. The microstructure was observed with a SEM Philips XL-30. The mechanical properties, elastic modulus, flexural strength, and fracture toughness, were measured in directly sintered prismatic bars (52 × 10 × 2.5 mm length, width and thickness respectively). The elastic modulus was measured by resonance with an Mk5 Industrial of GrindoSonic apparatus. The flexural strength and fracture toughness were measured by three point bend tests (25 mm span for flexural strength and 20 mm span for fracture toughness tests) in a universal materials testing of Instron, model 8501, with a load cell of 1 kN capacity. Crosshead displacements during the tests were measured with an LVDT strain gauge (resolution ± 1 μm). All the tests were run under displacement control at a loading speed of 50 μm/min; the load was applied with high purity alumina (99.7%) bars and cylinders. A straight notch, with 0.5 mm length and 80 μm notch radius, was introduced with a diamond saw in the specimens for fracture toughness test.

Three-point bending strength was determined by applying Bernoulli's theory, while design failure was calculated from the general equation for notched beams proposed by Guinea et al. [15]. In addition, the fracture surfaces of the samples tested were examined under a JEOL JSM 6300 scanning electron microscope.

3. Results and discussion

3.1. Sintering of samples with the higher powder loading

Fig. 2 shows the evolution of the XRD patterns with sintering temperature for uniaxially compacted parts. The starting powder presents the main peaks of the Ni-Zn ferrite spinel phase and the most intense peaks of Fe_2O_3 (stars in Fig. 2), indicating that most of the initial powder is the spinel. At sintering temperatures lower than 1250 °C some peaks remain which are associated to Fe_2O_3, and only in the XRD pattern for the sample sintered at 1250 °C can all the diffraction peaks be indexed using only the spinel crystal structure. This indicates that full reaction took place allowing the formation of the ferrite phase at 1250 °C. The unit cell parameters refined from the XRD patterns were a = 8.3925 Å, in good agreement with the reported value [14].

Fig. 3 shows the evolution of density as a function of sintering temperatures of injected samples with the higher loading powder

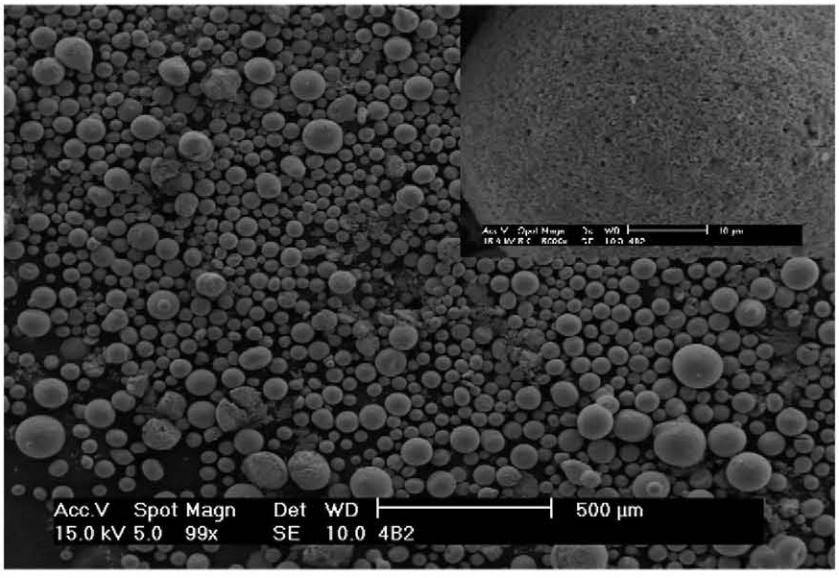

Fig. 1. Scanning electron microscopy images of Ni–Zn ferrite powder as received. Inset shows a magnified sphere.

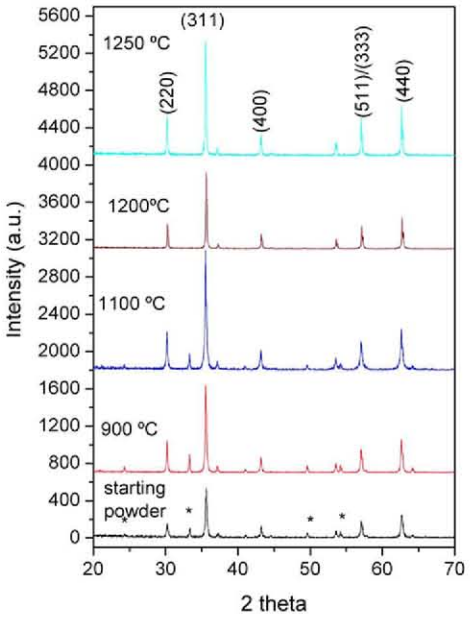

Fig. 2. X-ray diffraction pattern of starting powder and powder sintered at different temperatures.

(58% volume) and uniaxially pressed samples. In both samples the density increases almost linearly with the sintering temperature. However the sintered density of PIM samples is always higher than those of the uniaxially compacted specimens; theoretical densities higher than 90% were achieved at temperatures above 1200 °C. At the highest sintering temperature, 1300 °C, considerable grain growth was observed, indicating a clear oversintering, suggesting that unlike other ceramic systems, the characteristic plateau found in the sintering curves do not appear for Ni-Zn ferrites. Temperatures higher than 1300 °C were not tested due to the possibility of Zn losses as reported elsewhere [16].

Microstructures of cross-section of both samples (PIM with 58% in vol. powder loading and uniaxially compacted) at different sintering temperatures are shown in Fig. 4. The black contrast areas correspond to pores while bright areas correspond to ferrite grains. As shown, the sintering temperature has great influence on the microstructure of both samples. Porosity decreases significantly with increasing sintering temperature. Alternatively, the micrographs show that the average grain size increases with sintering temperature. This growth is roughly homogeneous in the case of PIM samples, while in the case of compacted sample is more heterogeneous.

3.2. Magnetic properties with maximum powder loading

Fig. 5 shows the evolution of the PIM (58% loading powder) and uniaxial samples permeability as a function of sintering temperature. Measurements were performed at 10 kHz on sample with toroidal shape. As expected, the permeability increases with the sintering temperature, though two different behaviours were found. Up to 1100 °C the permeability slightly increases with both samples (PIM and uniaxially compacted specimens) presenting the same values for each sintering temperature. The microstructural study revealed that up to this temperature the grain growth did not occur and the increased density could be correlated with the reduction of porosity; in Fig. 4 we can observe that at 1100 °C grain size in both samples show similar microstructures. Above this temperature, grain growth occurs and the initial permeability increases considerably. This increase is more significant in the case of PIM samples, since the average grain size is higher and also because the presence of pores decreases the permeability value appreciably. This effect has been also observed by Mahmud et al [17], who demonstrated that the permeability decreased as grain size increases in samples with high porosity. In both PIM and uniaxially pressed samples, the optimum sintering temperature was 1250 °C since grain growth was observed at higher temperatures.

Fig. 6 shows the relative loss factor, i.e. the ratio of the magnetic loss tangent (tan δ) to initial permeability (μ). For high-frequency magnetic applications, high μ and low tan δ are required. As shown in Fig. 6, the relative loss factor of the material processed at 1250 °C is slightly higher in lower frequency range. This fact is attributed to higher permeability losses as a consequence of the porous structure of the material. Similarly, these losses are higher in the case of the compacted samples as a consequence of the higher porosity (about 14% versus 8%). It is well known that hysteresis loss increases with increased porosity [18]. Finally, we must emphasize that the values of relative loss factor found in the PIM are quite suitable for high frequency applications.

3.3. Effect of powder loading on the mechanical behavior

The sintering process for the materials analyzed in this section was carried out in air at 1250 °C for two hours because this temperature

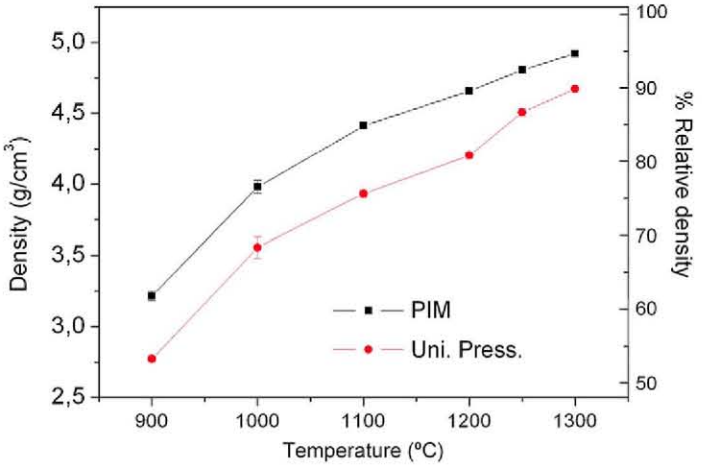

Fig. 3. Variation in density with sintering temperature of PIM (■) and compacted samples (●).

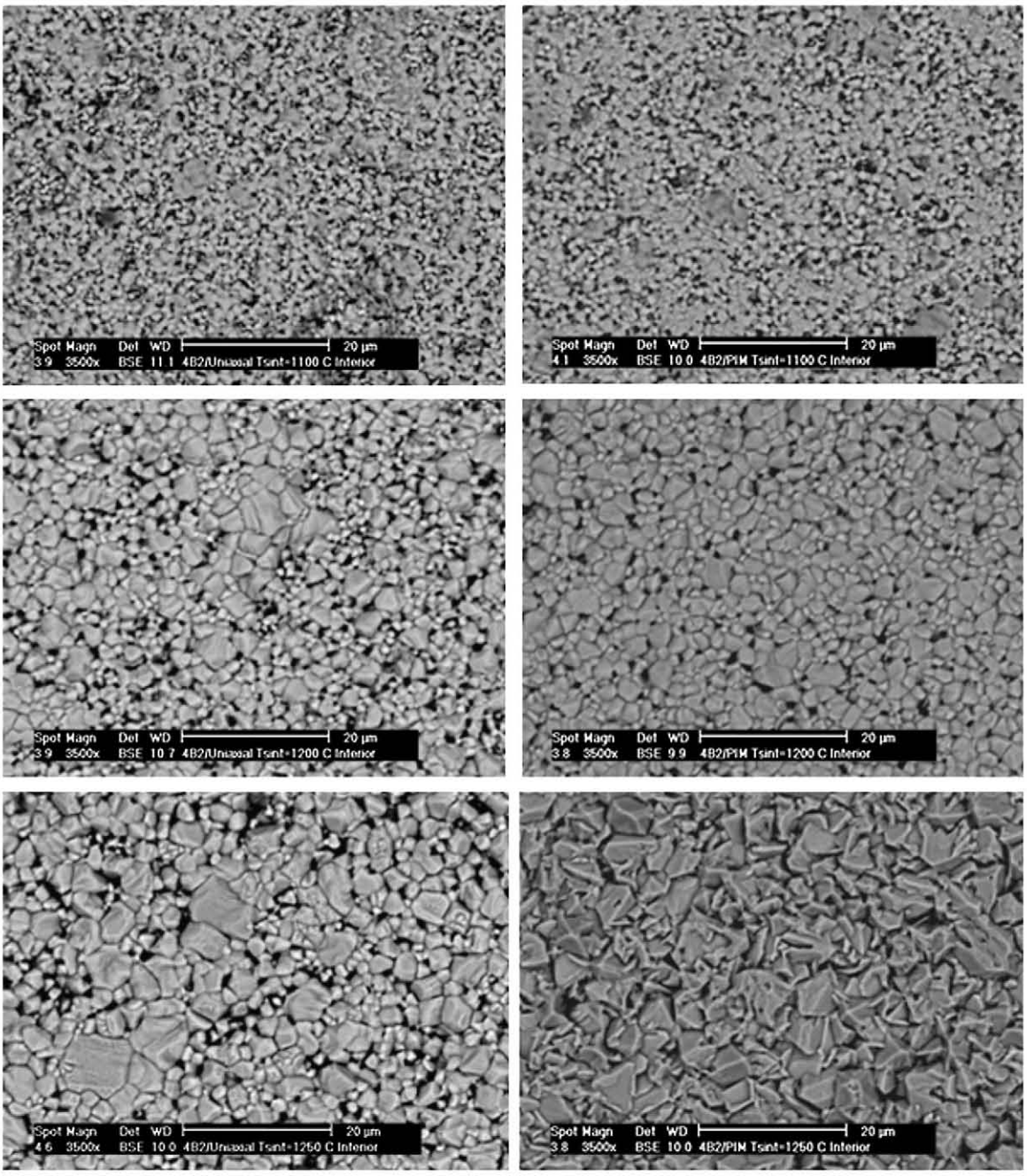

Fig. 4. Microstructure of sintered compact (uniaxial pressing left and PIM right) at different temperatures (1100 °C, 1200 °C and 1250 °C).

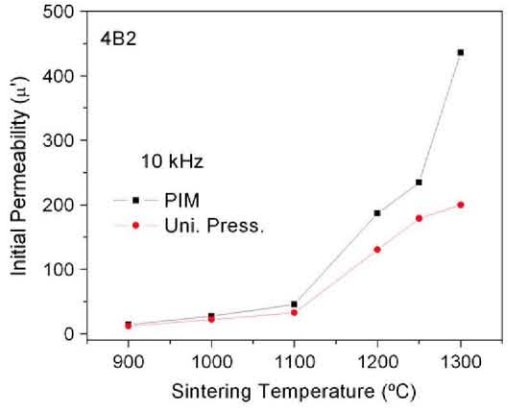

Fig. 5. Variation of initial permeability with sintering temperature.

turned out to be the most adequate, in order to increase bulk density and limit grain growth.

As is well known, porosity has a strong influence on mechanical properties. In order to determine the influence of powder loading on the density (porosity) and mechanical properties, we obtained one sample by uniaxial compaction (reference) and three, with different powder loading (52, 55 and 58% in vol.) by injection moulding. As shown in Fig. 7, PIM specimens had higher densities than the uniaxially pressed sample, and the maximum density was achieved for sample with a powder loading of 55% volume. In general, an increase in powder loading results in a decrease in porosity. The observation that samples with a powder loading of 58% present a slightly lower density could suggest that maximum powder loading has been exceeded. However, Powder Injection Moulding technology requires feedstock with high powder loading in order to achieve the highest performances.

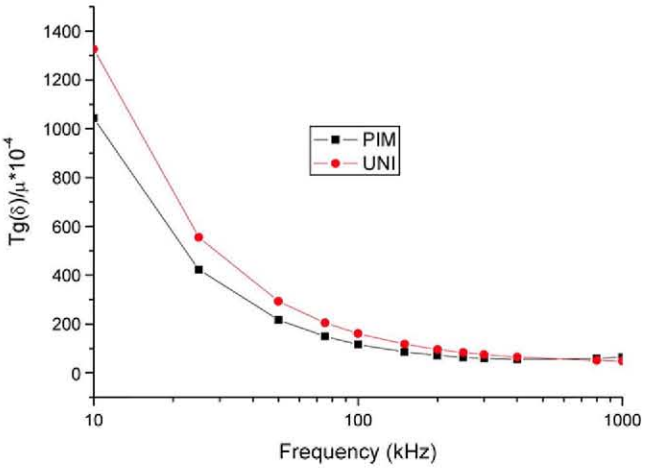

Fig. 6. Loss factor with frequency of toroid parts processed by PIM and uniaxial pressure and sintered at 1250 °C.

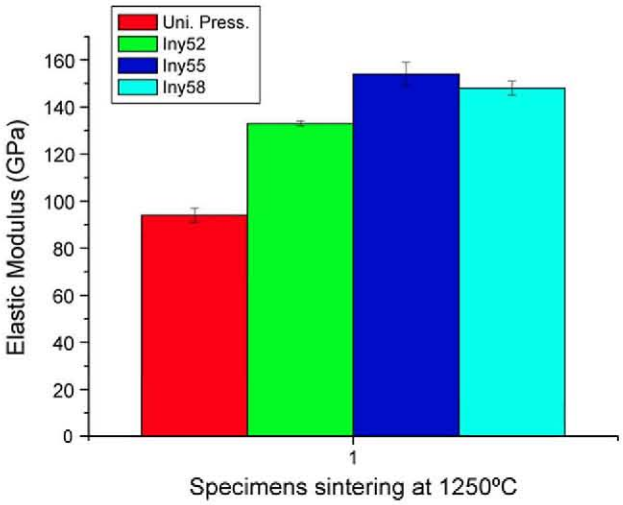

Fig. 8. Variation of elastic modulus with powder loading and fabrication technique.

Fig. 8 shows the variation of elastic modulus for PIM samples with different powder loading. The data are compared with that of the specimen prepared by uniaxial compaction. A good correlation between density of the sintered bulk material and elastic modulus was found. Maximum elastic modulus values were achieved for PIM samples with 55% powder loading. Even in PIM samples with similar density value to uniaxial compacted sample, the difference in elastic modulus is 30%. This fact could be related to PIM samples being more isotropic.

Figs. 9 and 10 show the variation of flexural strength and fracture toughness, respectively, of sintered specimens as a function of powder loading and fabrication technique. The flexural strength and toughness decreased with increasing powder loading. The PIM specimens with a powder loading of 52% and 55% have higher values than uniaxially pressed samples. These kinds of studies are scarce [19], and normally the mechanical properties increase with powder loading and it could be related to the optimum powder loading, which in our case was achieved for 55%.

Two relevant facts can be seen, the first is that PIM-sample with a powder loading of 52% enhanced the flexural strength and fracture toughness by *ca.* 50% compared with the material processed by uniaxial compaction. This is a significant improvement, and cannot be justified only by a slight increase in the density of the bulk material. In contrast, the flexural strength and the fracture toughness decrease when the powder loading is increased. This drop is so large for the material with 58% powder loading that the flexural strength is even lower than that of the compaction specimen. In order to understand the results obtained from the mechanical characterization, the fracture surfaces of the broken specimens of all the materials tested were analyzed by scanning electron microscopy. In this way we have tried to correlate the microstructural aspects with the macroscopic mechanical behaviour of the materials.

For uniaxial compaction material it can be seen, Fig. 11, that due to the sintering process there are small (about 1 μm) holes and cavities of a size around 20–25 μm. Additionally, in this case the fracture is mainly intergranular, since the grains are not well linked and each is surrounded by micropores. Both factors are responsible for the poor mechanical properties of this material.

In Fig. 12 it can be observed that in some cases pointed cavities appear, in which cracks are generated from the sharp corners, which also contribute to limit the mechanical properties of the compacted material.

PIM samples with 52 vol.% powder loading (Fig. 13) exhibit improved sintering behavior, with a more uniform distribution of smaller cavities (around 4 microns). Also, the microporosity between grains is reduced and the grain size is significantly smaller than for uniaxially compacted specimens. All these factors contribute to increased fracture toughness and flexural strength. Finally, as in the previous case, the fracture mode is mainly intergranular.

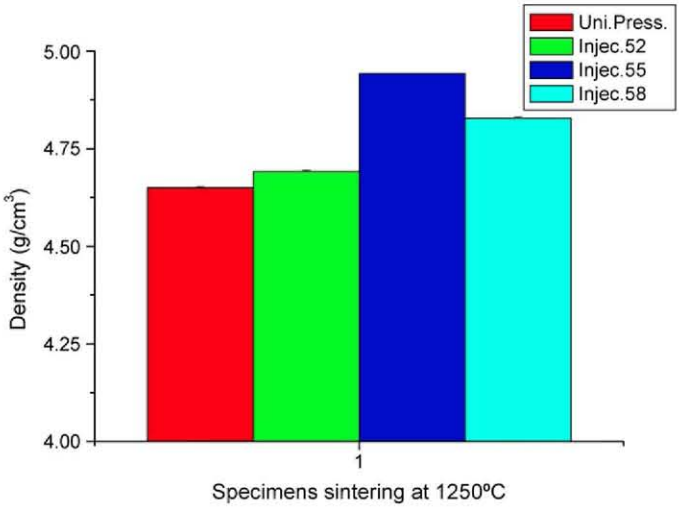

Fig. 7. Evolution of density with powder loading of PIM sample. Data are compared with that of the uniaxial compacted samples.

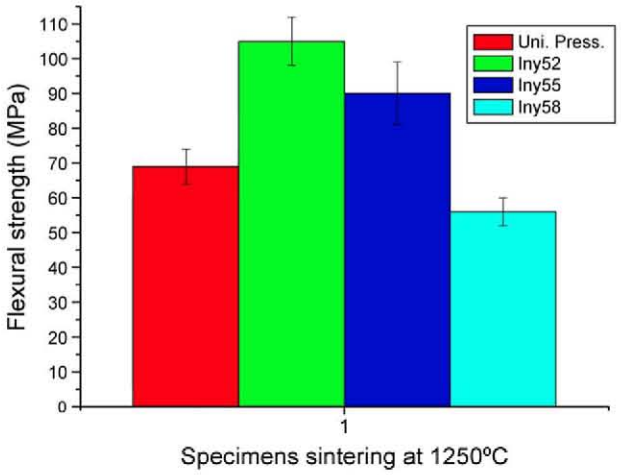

Fig. 9. Variation of flexural strength with powder loading and fabrication technique.

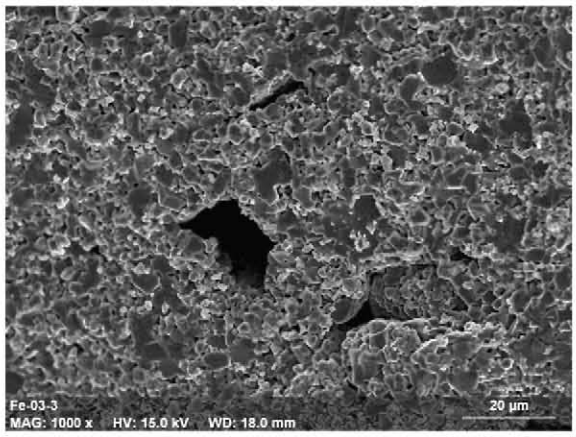

Fig. 11. Fracture surface of a compact sample.

For PIM samples with 55 vol.% powder loading (Fig. 14) a bimodal distribution of the grains was observed. In addition to small grains, a little bigger than in the 52% material, big grains (over 40 µm) can also be seen. While the small grains exhibit again an intergranular fracture mode, the big grains present a transgranular fracture mode, and in fact they appear to be working as critical defects of the material. These big grains appear poorly bonded to those around them and contain a significant number of small pores. The latter is consequence of their origin; these grains have been formed from the merging of smaller grains. Some of the pores surrounding the small grains could not be eliminated during the sintering process and they have been trapped in the merged grain. Consequently we think that these big grains are responsible for the reduced mechanical properties in this material.

Finally, in the PIM samples with 58% vol. powder loading (Fig. 15) a fractography very similar to the uniaxial compaction material was observed: cavities and holes with sizes over 10–15 µm very localized and close between them, poorly compacted zones, and grains that are poorly bonded with abundant microporosity around them. On the other hand, it was also found (Fig. 16) that there are quite long flaws due to the sintering process perpendicular to the fracture surface. In some cases these flaws almost cross the complete fracture surface. All these facts contribute to the sharp drop in mechanical properties, to similar or lower values than those obtained by uniaxial compaction.

4. Conclusions

A systematic sintering study of Ni–Zn ferrite specimens obtained by PIM and uniaxial compaction has been carried out. Samples obtained by both manufacturing processes present similar sintering curves; however the highest densification is achieved for samples processed by PIM where compacts with theoretical density as high as 95% were obtained. In both cases the optimum sintering temperature was 1250 °C; at higher temperatures significant grain growth was observed. The microstructure study showed that grain size increases with sintering temperature. In the case of uniaxially compaction heterogeneous grain growth were observed, and the presence of significant porosity even at the highest temperature was detected. In the case of PIM sample the grain growth was homogeneous and the presence of porosity was scarce at higher temperatures.

A very good correlation between magnetic properties, bulk densities and microstructures was found. At low sintering temperatures, samples processed by both methods present similar initial permeabilities as a consequence of similar porosity and grain size, while at temperatures higher than 1100 °C the permeability considerably increases, particulary in PIM samples due to the considerably decreased porosity. The values of relative loss factor found in the PIM and uniaxially compacted samples are quite suitable for high frequency applications, though these losses were lower in PIM samples.

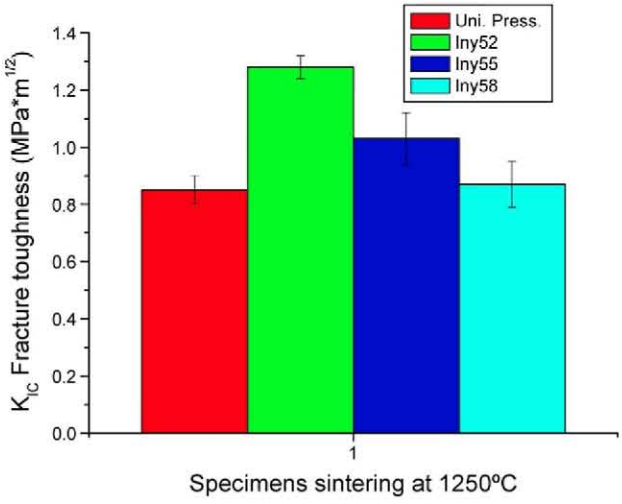

Fig. 10. Evolution of fracture toughness with powder loading and fabrication technique.

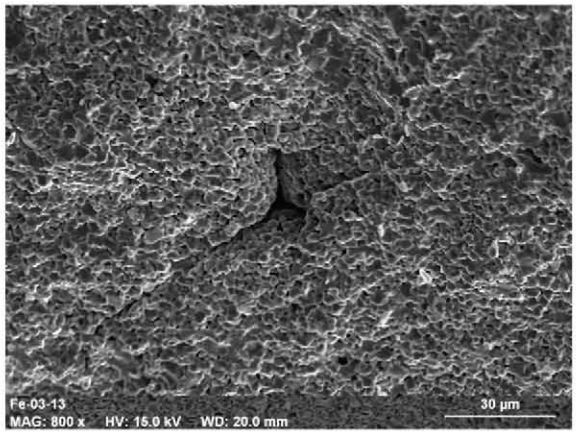

Fig. 12. Detail of the sharp cavities in a compact sample, where cracks are generated from their corners.

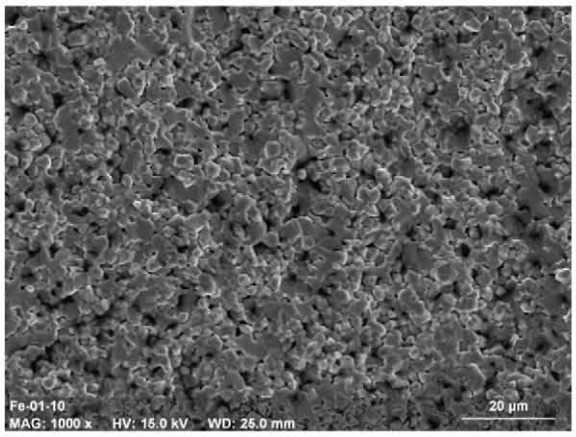

Fig. 13. Fracture surface of a material processed by PIM with 52% powder loading.

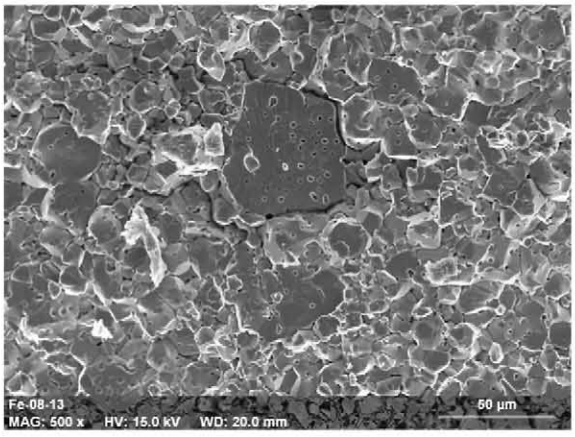

Fig. 14. Fracture surface of a material processed by PIM with 55% powder loading. Notice the large size of some grains, and how they are decohesive from the rest of the grains.

Regarding mechanical behaviour, we have found a very good correlation between density and elastic modulus. PIM samples present higher density and elastic modulus compared with uniaxially compacted samples. These properties are enhanced with powder loading, with a maximum value obtained for samples with a powder loading of 55%.

In the case of flexural strength and fracture toughness, the best results were obtained for PIM samples with 52% powder loading. The improvement in these properties is excellent, reaching 150% over the reference material. Nevertheless, both properties decreased strongly with increased powder loading since this generated a bimodal grain distribution (55% vol.) and increases in pore size and number of cavities (58% vol.), which degrade the mechanical behaviour.

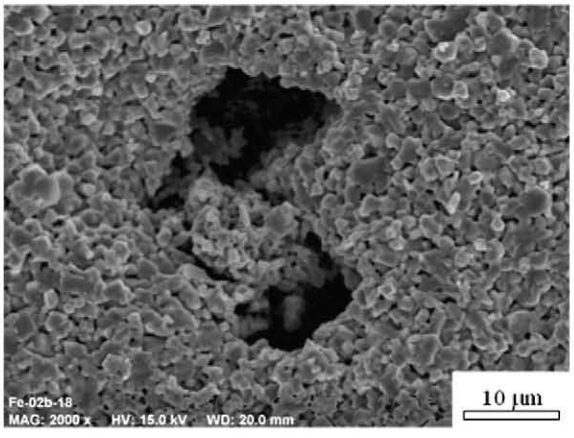

Fig. 15. Fracture surface of a material processed by PIM with 58% powder loading.

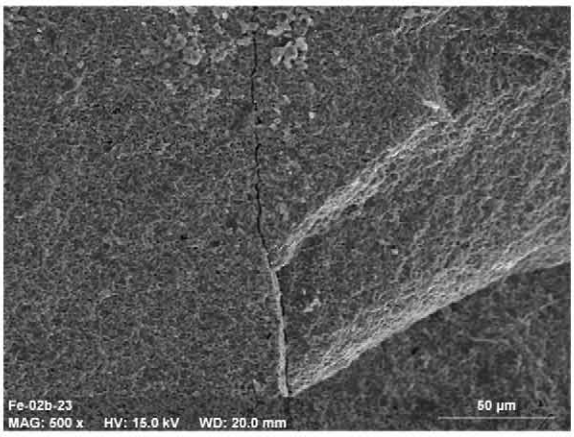

Fig. 16. Flaws in a PIM part with 58% powder loading.

In summary, the powder injection moulding method has been successfully applied to the production of Ni–Zn ferrites. Furthermore, the magnetic and mechanical properties were clearly improved.

Acknowledgements

The authors thank Spanish Agency CICYT (MAT2007-29278-E, MAT2007-64486-C07-06 and MAT2010-19837-C06-05 projects) and Regional Government of Madrid (Project ESTRUMAT S-0505/MAT/0077 and MATERYENER S2009 PPQ 1626) for financial support.

References

[1] R.M. German, A. Bose, Injection molding of metals and ceramics, MPIF, NJ USA, 1997.
[2] R.M. German, Powder Injection Molding, MPIF, Princenton, NJ USA, 1990.
[3] P. Thomas-Vielma, A. Cervera, B. Levenfeld, A. Várez, Journal of the European Ceramic Society 28 (2008) 763–771.
[4] D.S. Tsai, W.W. Chen, Ceramics International 17 (1995) 79–87.
[5] S.T. Lin, R.M. German, Journal of Material Science. 29 (1994) 2752–5207.
[6] M. Trunec, P. Dobsak, J. Cihlar, Journal of the European Ceramic Society 20 (7) (2000) 859–866.
[7] T. Jardiel, B. Levenfeld, R. Jimenez, A. Várez, Ceramics International 35 (2009) 2329–2335.
[8] S. Lin, Ceramics International 27 (2) (2001) 205–214.
[9] A.J. Pigram, R. Freer, Journal of Magnetism and Magnetic Material 29 (1994) 6420–6426.
[10] E. Rodríguez-Senin, B. Levenfeld, A. Varez, J.M. Torralba, M.A. Paris, Powder Metallurgy 48 (3) (2005) 249–253.
[11] N. Murillo, J. Gonzalez, C. Guraya, M. Gutierrez, F.J. Seco, Journal of Magnetism and Magnetic Material 203 (1–3) (1999) 165–168.
[12] E.C. Milke, M. Rei, J. Palgi de Soze, L. Schoeffes, International Journal of Powder Metallurgy 37 (3) (2001) 47–51.
[13] L.A. Dobrzanski, G. Matula, A. Várez, B. Levenfeld, J.M. Torralba, Journal of Materials Processing Technology 157–158 (2004) 658–668.
[14] A. Goldman, Modern ferrite Technology, Ferrite Technology Worldwide, Inc, Van Nostrand Reinhold, 1990.
[15] G.V. Guinea, J.Y. Pastor, J. Planas, M. Elices, International Journal of Fracture 89 (1998) 103–116.
[16] A. Dias, R.L. Moreira, Material Letters 39 (1999) 67–76.
[17] S.T. Mahmud, A.K.M. Akther Hossain, A.K.M. Abdul-Hakim, M. Seki, T. Kawai, H. Tabata, Journal of Magnetism and Magnetic Materials 305 (2006) 269–274.
[18] L. Neel, Annales de Physique 3 (2) (1948) 137–198.
[19] K.A. Khalil, S.W. Kim, Metals and Materials International 12 (2) (2006) 101–106.